Supporting Information

Static and dynamic structural probing of swollen polyacrylamide ferrogels

J.A. Galicia[1,2], F.Cousin[3], E. Dubois[1], O. Sandre[1], V. Cabuil[1], R. Perzynski[1,*]

[1] UPMC Univ Paris 6 – Laboratoire PECSA – UMR 7195 CNRS – UPMC – ESPCI, case 51, 4 Place Jussieu, 75252 Paris cedex 05 – France
[2] Fac. de Ing. Quimica, Benemerita Universidad Autonoma de Puebla, Edif 147/102 Ciudad Universitaria,18 sur y San Claudio, Puebla, Pue. Mexico
[3] Laboratoire Léon Brillouin, UMR 12 CNRS-CEA, CEA-Saclay, 91191 Gif-sur-Yvette - France

* corresponding author

e-mail : regine.perzynski@upmc.fr

1 Hydrogels

1.1 - Synthesis

The hydrogels are obtained by free radical polymerization as described in part 3a of the main article replacing the ferrofluid by an aqueous solution of trisodium citrate (Na_3Cit) at a concentration 8.10^{-3} mol.L^{-1}. The range (0.5-2%) of cross-linker ratio is chosen for the following reasons:
(i) Below CL = 0.5%, the gels are too soft to be manipulated
(ii) Above CL = 2%, PAM hydrogels are known to present local heterogeneities of cross-linkers.[1,2,3]

1.2 Swelling of the hydrogel

At the end of the synthesis, the hydrogel is out of thermodynamical equilibrium. Placed inside a water bath at the same concentration [Na_3Cit] as the synthesis medium, it absorbs a large volume of water. The swelling equilibrium is reached when the hydrogel mass does not evolve anymore (typically after 3 weeks). Before reaching equilibrium, the bath is changed several times in order to accelerate the equilibration process. When equilibrium is reached, the swollen gel is weighed ($m_{swollen}$), then dried at 70°C during 12 hours, and weighed again (m_{dried}). m_{dried} is very close to the mass of polymer $m_{polymer}$ because the polymerization yield is measured equal to 98%. This allows to determine the swelling ratio G_{HG}^{equil} at equilibrium through $(m_{swollen} - m_{dried})/m_{polymer} = m_{H_2O}/m_{polymer}$. G_{HG}^{equil} depends on the degree of cross-linking CL (see Table S1). It is related to the volume ratio of polymer at equilibrium through $\varphi_{AM}^{equil} = \rho_{H_2O}/\rho G_{HG}^{equil}$ with ρ/ρ_{H_2O} = 1.35, ρ being the polymer density. The same formula stands at the end of the synthesis: $\varphi_{AM}^{synth} = \rho_{H_2O}/\rho G_{HG}^{synth}$ where φ_{AM}^{synth} and G_{HG}^{synth} are the volume ratio of polymer and the swelling ratio in the preparation state (after cross-linking and before swelling).

1.3 –Swelling pressure of hydrogels and mesh size of the hydrogel polymeric array

Once G_{HG}^{equil} is measured, it is possible to calculate the initial swelling pressure Π_{swl}^{HG} (at polymer volume fraction $\varphi_{AM} = \varphi_{AM}^{synth}$) following Flory-Rehner theory knowing the Flory parameter χ. It is also possible to calculate the number of monomers N_C between two cross-links and to estimate the mesh size of the polymeric network ξ_{equil} either from the volume density of cross-links or from the gyration radius of a polymer branch between two cross-links that gives very similar results. All the results are summed up in Table S1 for the three cross-linking ratios CL used here.

CL (%)	G_{HG}^{synth}	φ_{AM}^{synth} (%)	G_{HG}^{equil}	φ_{AM}^{equil} (%)	$N_c = M_c/M$	ξ_{equil} . ξ_Θ (nm)	ξ_{synth} (nm)	Π_{swl}^{HG} (kPa)
0.5	25.9	2.78	74.4	0.99	1.5510^3	24.0, 23.0	16.8	3.60
1	25.4	2.83	54.0	1.35	$8.3\ 10^2$	17.5, 16.5	13.4	3.52
2	24.9	2.88	38.9	1.87	$4.2\ 10^2$	12.5, 12.0	10.8	2.93

Table S1- ***Characteristics of the hydrogels*** – CL cross-linking ratio; G_{HG}^{synth} and φ_{AM}^{synth} : swelling ratio and polymeric volume ratio of the hydrogel determined immediately after synthesis; G_{HG}^{equil} and φ_{AM}^{equil} : swelling ratio and polymeric volume ratio at swelling equilibrium; N_c is the number of monomers between two cross-links, M_c being the molar mass of polymer between cross-links deduced at equilibrium from eqn (S4) and M the molar mass of monomer AM; ξ_{equil} is the mesh size of the hydrogel at swelling equilibrium deduced from eqn (S5), ξ_Θ the mesh size of PAM in a Θ solvent; ξ_{synth} is the mesh size of the hydrogel immediately after synthesis, Π_{swell}^{HG} the initial swelling pressure of the hydrogel at $\varphi_{AM} = \varphi_{AM}^{synth}$.

The thermo-dynamical equilibrium of a neutral polymeric array, with a homogeneous distribution of reticulation nodes is ruled by a balance between osmotic and elastic forces. The swelling pressure of the hydrogel Π_{swl} is given by [4,5] :

$$\Pi_{swl}^{HG} = -\frac{1}{V_1}\left(\mu_1^{gel} - \mu_1^{bath}\right) = \Pi_{mix}^{HG} - \Pi_{el}^{HG} \qquad \text{(SI.1)}$$

where μ_1^{gel} (resp. μ_1^{bath}) is the chemical potential of water inside the hydrogel (resp. inside the bath), V_1 is the molar volume of the aqueous solvent (= 18 cm^3/mol), Π_{mix}^{HG} is the contribution coming from entropic and enthalpic effects due to the polymer/solvent mixing, Π_{el}^{HG} is the elastic pressure associated to the stretching of the polymeric chains with respect to their reference molten state (without solvent). We forget here any contribution coming from electrostatic interactions between chains (see end-note (*)). The mixing pressure writes:

$$\Pi_{mix}^{HG} = -\frac{R_o T}{V_1}\left(\ln(1-\varphi_{AM}) + \varphi_{AM} + \chi\varphi_{AM}^2\right)$$

$$\cong \frac{R_o T}{V_1}\left(\frac{1}{2} - \chi\right)\varphi_{AM}^2 \quad \text{if } \varphi_{AM} << 1 \qquad \text{(SI.2)}$$

where R_o is the Perfect Gas constant, T the temperature in Kelvin, φ_{AM} the volume fraction of polymer inside the hydrogel and χ the Flory parameter which is here equal to 0.47.[6,7]

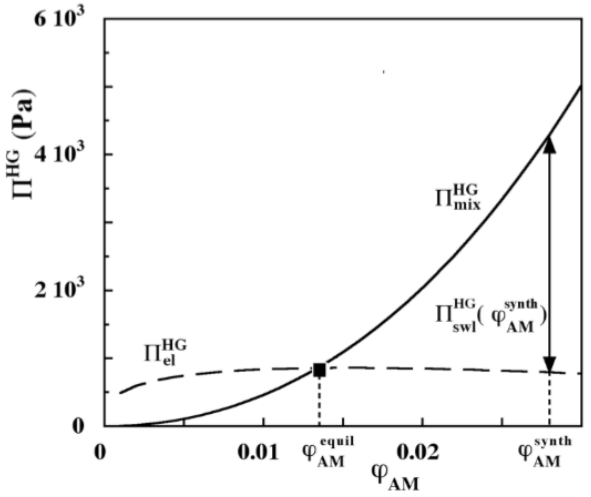

Figure S1 – ***Various pressures of hydrogel and elastic modulus*** – Mixing pressure Π_{mix}^{HG} (eqn (S2) - full line) and elastic pressure Π_{el}^{HG} (eqn (S3) - dashed line) as a function of the polymer concentration φ_{AM}. In the synthesis conditions, $\varphi_{AM} = \varphi_{AM}^{synth}$ and the swelling pressure $\Pi_{swell}^{HG} = \Pi_{mix}^{HG} - \Pi_{el}^{HG}$. At swelling equilibrium, $\varphi_{AM} = \varphi_{AM}^{equil}$ and $\Pi_{mix}^{HG} = \Pi_{el}^{HG}$ (solid square). It is proportional to the elastic modulus of the swollen hydrogel at equilibrium. A coefficient 0.67 is found while comparing to the measurement at CL = 1% of ref [8].

The elastic contribution is related to the entropy of the stretched chains. Supposing an isotropic swelling with a homogeneous distribution of nodes in the hydrogel, we obtain :

$$\Pi_{el}^{HG} = R_o T \nu_c \left[\varphi_{AM}^{synth} \left(\frac{\varphi_{AM}}{\varphi_{AM}^{synth}} \right)^{1/3} - \frac{1}{2} \varphi_{AM} \right] \qquad \text{(SI.3)}$$

where $\nu_c = \rho / M_c$ is the volume concentration of nodes in the dry hydrogel (in mol/vol. of polymer), M_c being the molar mass between cross-links.

When the system is out of equilibrium, eqn (S1) governs the swelling of the hydrogel. Figure S1 illustrates the φ_{AM}-dependence of Π_{mix}^{HG} (full line) and Π_{el}^{HG} (dashed line) at CL = 1%. Just after synthesis, Π_{mix}^{HG} given by eqn (S2) with $\varphi_{AM} = \varphi_{AM}^{synth}$ is much larger than $\Pi_{el}^{HG}\left(\varphi_{AM}^{synth}\right)$ as it corresponds to a deformation still small with respect to the melt. In that case, because Π_{swl}^{HG} is positive, the hydrogel absorbs water from the swelling bath. As the hydrogel swells, φ_{AM} decreases, Π_{mix}^{HG} decreases and Π_{el}^{HG} slightly increases, the hydrogel swells less and less. When $\Pi_{swl}^{HG} = 0$, that is when $\Pi_{mix}^{HG} = \Pi_{el}^{HG}$, the equilibrium is reached, $\varphi_{AM} = \varphi_{AM}^{equil}$ and the swelling stops.

The volume fraction of polymer inside the hydrogel at the end of the synthesis is almost the same for all the samples, the slight variation in Table S1 resulting from the different CL. The volume ratio φ_{AM}^{equil} is deduced from the measurement of the swelling ratio G_{HG}^{equil}. It allows obtaining M_c at equilibrium (see Table S1) through:

$$M_c = V_1 \rho \frac{\left[\frac{1}{2} \varphi_{AM}^{equil} - \varphi_{AM}^{synth\,2/3} \varphi_{AM}^{equil\,1/3} \right]}{\ln\left(1 - \varphi_{AM}^{equil}\right) + \varphi_{AM}^{equil} + \chi \varphi_{AM}^{equil\,2}} \qquad \text{(S4)}$$

We can thus deduce the number of monomers $N_c = M_c / M$ between two cross-links, M = 71 g/mol being the molar mass of monomer AM. We obtain also the mesh size ξ_{equil} at swelling equilibrium from:

$$\xi_{equil} = \left[N_a \nu_c \varphi_{AM}^{equil} \right]^{-1/3}. \qquad \text{(S5)}$$

Let us note that the state of the system being close to Θ conditions (χ = 0.47 ~ 1/2) the mesh size ξ_{equil} at swelling equilibrium is closer to $\xi_\Theta = aN^{1/2}$ than to the Flory mesh size $\xi_F = aN^{3/5}$, a = 0.58 nm being the length of monomer AM.[9,10]

The experimental evidence that the structure of hydrogels is homogeneous (in the synthesis conditions and at swelling equilibrium) is provided by the fact that the effective concentration of cross-links at swelling equilibrium (~ $1/N_c$) is found proportional to CL. The mesh size after the synthesis is here given by $\xi_{synth} = \xi_{equil} \left(G_{HG}^{synth} / G_{HG}^{equil} \right)^{1/3}$.

2 Ferrofluids

2.1 Synthesis

The magnetic nanoparticles are synthesized by co-precipitation in an aqueous ammonia solution of $FeCl_2$ and $FeCl_3$ salts that leads to colloidal magnetite which is fully oxidized to maghemite by $Fe(NO_3)_3$ in acidic medium.[11] The experimental conditions have been chosen in order to prepare particles with an average diameter of the order of 6-12 nm. A size-sorting process allows then a fractionation of the population of nanoparticles according to their diameter.[12] Finally the initially positively charged nanoparticles are coated with citrate species by addition of tri-sodium citrate (Na_3Cit) in order to have negative surface charges associated to ionized carboxylate groups for pH ranging between 6 to 10. The citrate coated particles yield to stable dispersions in water at pH 7, the electrostatic inter-particle repulsion preventing the nanoparticle aggregation. The adsorption equilibrium of citrate gives a residual ionic strength due to unadsorbed (free) citrate species Cit^{3-} and their Na^+ counterions. To ensure the citrate coating, one needs to keep free citrate salt concentration [Na_3Cit] above a given minimal value, which depends on pH.[13] At pH 7, the adsorption plateau corresponds to a free citrate concentration inside the solution [Na_3Cit] ≥ 2. 10^{-3} mol.L^{-1}.

2.2 SANS experiments :

The size and structure of FFA and FFB dispersions have been determined by SANS experiments performed at the LLB facility (CEA-Saclay, France) on the PAXY spectrometer, in the wave-vector range 0.0065 Å^{-1} ≤ q ≤ 0.15 Å^{-1}. In pure light water, the intensity after subtraction of the incoherent background is largely dominated by the nuclear contribution of the particles.[14] The intensity I(q,Φ) scattered by the dispersion of roughly spherical nanoparticles at volume fraction Φ writes:

$$\frac{I(q,\Phi)}{\Phi} = \Delta\rho^2 F(q) S(q,\Phi) \qquad \text{(S6)}$$

where $\Delta\rho^2$ = 5.67 10^{21} cm^{-4} is the neutron nuclear contrast of the nanoparticles with respect to H_2O, *F(q)* is the form factor of the nanoparticles and *S(q,Φ)* the structure factor of the colloidal dispersion. In the dilute regime and if the inter-particle interactions are negligible, the structure factor of the dispersions is equal to 1. The scattered intensity is then proportional to *F(q)*.

Figure S2a presents the SANS scattered intensity (divided by Φ) for sample FFB at various Φ and low ionic strength [Na_3Cit] = 8.10^{-3} mol.L^{-1}. The intensity at Φ=0 is proportional to *F(q)* and gives the size and shape characterization deduced from such an experiment. The plateau at low q in the Guinier range (q < 2.10^{-2} Å^{-1}) obtained at the lowest volume fraction confirms that for Φ < 1%, the interactions between

nanoparticles can be almost neglected in the experimental conditions. At large q ($q > 6.10^{-2}$ Å^{-1}) in the so-called Porod regime, $I(q,\Phi)/\Phi$ roughly decreases as q^{-4} whatever Φ, which is characteristic of solid particles with a sharp interface. Figure S2a presents the best fit of the form factor of the FFB particles, assumed spherical with a lognormal distribution of median diameter d_O^{scat} = 7 nm and polydispersity σ^{scat} = 0.26 (see Table S2 for FFA characteristics).

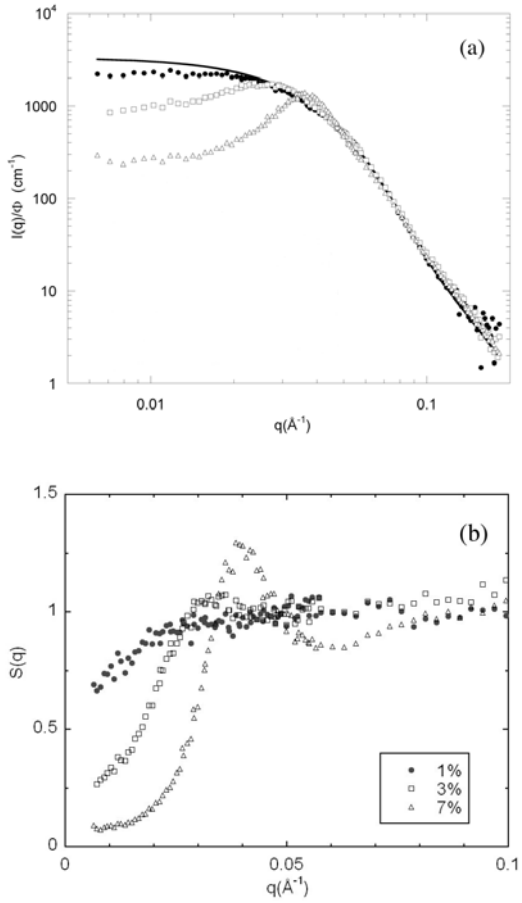

Figure S2 ***SANS probing of FFB ferrofluids at various Φ*** - The solid line is the form factor of the nanoparticles (see text and Table 2).
(a) Reduced scattering intensity I(q, Φ)/ Φ versus q at various Φ;
(b) Structure factor of the nanoparticles S(q, Φ) versus q at various Φ.

For volume fractions Φ > 1%, the inter-particle interactions are no longer negligible and the structure factor *S(q,Φ)* in eqn (S6) is no more equal to 1. Figure SI 2.b provides the structure factor *S(q,Φ)* of three dispersions at volume fractions Φ = 1%, 3% and 7%, based on the same nanoparticles (FFB) at $[Na_3Cit] = 8.10^{-3}$ mol.L^{-1}. In the thermodynamic limit (for $q \to 0$), the structure factor tends to the compressibility of the system. Figure 2 shows that it decreases as the volume fraction increases, which means that the inter-particle interaction is repulsive on average. The maximum of S(q) at q_{max}, associated to the most-probable distance $l_{mp} = 2\pi/q_{max}$ between scattering entities inside the dispersion, increases in amplitude and simultaneously moves towards higher q_{max} values. If the inter-particle interaction is repulsive on average, the nanoparticles are homogeneously dispersed inside the dispersion. Then the most probable distance $2\pi/q_{max}$ is also equal to the mean inter-particle distance l_{mean}, related to the volume fraction Φ of the dispersion and the median diameter d_0 of particles through $l_{mean} = d_o\sqrt[3]{\frac{\pi}{6\Phi}}$. For Φ = 3%, l_{mp} is ~ 196 Å (q_{max} ~ 0.032 Å^{-1}) and l_{mean} =212 Å. For Φ = 7%, l_{mp} is ~ 161 Å (q_{max} ~ 0.039 Å^{-1}) and l_{mean} is 160 Å. The good agreement between those two estimates in our ferrofluid dispersions shows that there are strong repulsive interaction between our nanoparticles at $[Na_3Cit] = 8.10^{-3}$ mol.L^{-1}.

	d_O^{scat} (nm)	σ^{scat}	d_O^{bir} (nm)	σ^{bir}	δn_o	τ_o (μs)	α	(nm)	δ (nm)
FFA	9.2	0.35	11.5	0.25	0.1	5.4	0.93	12	4.5
FFB	7.0	0.26	9.1	0.2	0.07	1.8	0.95	11	5

Table S2 - ***Characteristics of the ferrofluid nanoparticles*** – Parameters deduced by an adjustment to a log-normal distribution of diameters, of SANS (d_O^{scat}, σ^{scat}) and static birefringence (d_O^{bir}, σ^{bir}) measurements; δn_o is the intrinsic anisotropy of the nanoparticles[15]; τ_o characteristic relaxation time and α stretched exponent are deduced from the stretched exponential adjustment of birefringence relaxation using eqn (S8); d average nanoparticle diameter and δ electrostatic screening length are deduced from a Carnahan-Starling adjustment of the Φ-dependence of ferrofluid osmotic pressure Π(Φ) as in [16].

2.3 Osmotic equilibrium of Ferrofluids

In the ferrofluid dispersions used here, the magnetic nanoparticles, due to their citrate coating, are in strong repulsive interaction. The osmotic pressure Π^{FF} due to the nanoparticle/solvent mixing can be described in terms of repulsive effective Hard-Spheres following the Carnahan-Starling formalism[16]:

$$\frac{\Pi^{FF} V}{\Phi\, kT} = \frac{1+\Phi+\Phi^2+\Phi^3}{(1-\Phi)^3} \qquad \text{(S7)}$$

where $V = \frac{\pi}{6} d^3$, d being an averaged nanoparticle diameter. In the limit $\Phi \to 0$, the right hand term is equal to 1 and eqn (S7) reduces to the Perfect Gas law, also valid in the limit of low Φ if the balance of inter-particle interaction is null (i.e. if the second virial of the osmotic pressure equals zero). Here the balance is repulsive and the repulsions are taken into account in the right hand term of eqn (S7) replacing Φ by an effective volume fraction Φ_{eff}, which includes the range of the repulsion.[16] Indeed the repulsion is strong enough to consider the nanoparticles as Hard-Spheres with an effective diameter d + 2δ, where δ is the electrostatic screening length. It leads to an effective volume fraction $\Phi_{eff} = \Phi (1 + 2\delta/d)^3$. Figure 2 of the main text presents such fits for the two ferrofluids used here. We obtain d = 12 nm and δ = 4.5 nm for FFA (resp. d = 11 nm and δ = 5 nm for FFB).

2.4 - Magnetic and magneto-optical properties

Each nanoparticle bears a magnetic moment $\vec{\mu}$ which is of the order of 10^4 Bohr magnetons and an optical anisotropy axis $\vec{e}$. Its modulus $|\vec{\mu}| = m_S V_{magn}$ is proportional to the magnetic volume V_{magn} of the nanoparticles and to m_S the magnetization of the nanoparticles material. Under a large applied field $\vec{H}$, this magnetic moment $\vec{\mu}$ orientates along the field direction. In a liquid dispersion of 10 nm-sized γ-Fe_2O_3 nanoparticles, the magnetic torque also rotates mechanically the core of the nanoparticle together with its optical axis. At equilibrium in large fields, the optical axis $\vec{e}$ becomes parallel to $\vec{H}$. The alignment of $\vec{\mu}$ along $\vec{H}$ confers to the dispersion a macroscopic magnetization M. The alignment of the optical axis $\vec{e}$ of all the nanoparticles gives a macroscopic optical birefringence Δn to the dispersion. At saturation, all the magnetic moments and all the optical axes are aligned along $\vec{H}$, then $M = M_S = m_S\Phi$ and $\Delta n = \Delta n_S = \delta n_o \Phi$, δn_o being the

intrinsic optical anisotropy parameter of the nanoparticles.[17] For intermediate fields and low Φ's, M and Δn are well described by a Langevin's formalism with in particular $\Delta n = \Delta n_S L_2(\zeta)$, where $L_2(\zeta) = 1\text{-}3L(\zeta)/\zeta$, $L(\zeta) = \mathrm{ctanh}(\zeta)\text{-}1/\zeta$ and $\zeta = \frac{\mu_o \mu H}{kT}$ being respectively the Langevin's function and the Langevin's parameter. However, the shape of Δn(H) is modified by the size distribution of the nanoparticles.[17] In ferrofluids at low Φ's, the experimental measurements of magneto-optical birefringence as a function of the applied field enable the determination of $(d_O^{bir}, \sigma^{bir})$ by comparison to the theoretical Langevin formalism taking into account a log-normal size-distribution (see Table S2 and best fit of Δn(H) for FFA in fig.6).

The magneto-optical birefringence Δn(H) is measured as in [15] up to a few 100 kA/m. Figure 6 of main text presents the variations of Δn(H) normalized by its volume fraction Φ for a sample based on FFA nanoparticles at $[Na_3Cit] = 8.\ 10^{-3}$ mol.L^{-1} for Φ = 1% and the corresponding fit. The maximum value Δn_S of Δn is proportional to the volume fraction Φ, the proportionality coefficient δn_o being dependent on the nanoparticle size distribution.[15] The values of δn_o for FFA and FFB are given in Table S2. Figure 6 of main text presents also the reduced variations of $\Delta n(H)/\Delta n_S$ at Φ = 7%. The shape of the curve is almost independent on Φ in our range of volume fractions expressing the weak influence of inter-particle interactions on magneto-optical birefringence in the present repulsive regime.

The ferrofluid solutions can be also probed from a dynamic point of view. Using the same experimental device as the one described in [18], we analyze the optical rotational answer of the colloid to a pulse of magnetic field of small amplitude (H = 4.8 kA/m) and duration (~100 ms). The magnetic particles, being suspended in a liquid, align along the field direction during the pulse. It leads to a birefringence which, in low-field approximation, writes $\Delta n_{LF} = \delta n_O \Phi \zeta^2 / 15$. Here $\zeta \leq 0.14$ and Δn_{LF} is at most of the order of 10^{-5}. The temporal analysis of the birefringence relaxation at the cut-off of the field is performed in terms of a stretched exponential decay of optical intensity *I(t)* (see figure S3a):

$$I(t) = I_o e^{-\left(\frac{\tau}{\tau_o}\right)^{\alpha}} \qquad \text{(S8)}$$

with $I(t) \propto \sin\varphi$, φ being the (here time-dependent) phase-lag of the birefringent sample. We can determine three physical quantities: the initial intensity I_o, the characteristic relaxation time τ_o and the stretched exponent α. Providing that the phase-lag φ of the birefringent sample is small enough, the intensity I_o is proportional to Δn_{LF}. The condition $\varphi = 2\pi e \Delta n_{LF}/\lambda << 1$, where e is the thickness of the optical sample cell (here of the order of 100 μm) and λ the optical wave-length (here = 0.633 μm), is easily fulfilled ($\varphi \leq 10^{-2}$). Thus we obtain in the liquid suspension:

- for the intensity I_o of the magneto-optical pulse

$$I_o \propto \Phi \zeta^2 \propto \Phi V_{magn}^2 \qquad \text{(S9)}$$

- for the time τ_o, which is proportional to the characteristic time of rotational diffusion:

$$\tau_o = \frac{\eta V_H}{kT} \qquad \text{(S10)}$$

with η the viscosity of the liquid carrier and V_H the hydrodynamic volume of the nanoparticles.

- for the exponent α, which is related to the width of the distribution of relaxation times in the dispersion

$$\alpha \approx 1 \qquad \text{(S11)}$$

for samples based on nanoparticles of thin distribution of sizes. This α value is decreasing towards 0.6 in polydisperse or agglomerated liquid dispersions[18,19] and may reach a value of 0.3 in arrested thixotropic gels[18] or glass-forming systems[19].

The stretched-exponential nature of the relaxation of the magneto-optical signal is illustrated in the inset of figure S3a for sample FFA at Φ = 3% and $[Na_3Cit] = 8.\ 10^{-3}$ mol.L^{-1}. The almost linear variation of $-\ln(I/I_o)$ as a function of time t in this log-log representation, shows that there is only one stretched exponential relaxation process involved in the decay of intensity. The adjusted straight line crosses the horizontal axis $-\ln(I/Io) = 1$ at $t = \tau_o = 5.4$ μs. It has a slope α = 0.93. In our range of Φ and within our experimental accuracy, this relaxation time is found here independent of Φ. Table S2 gives τ_o (denoted τ_o^{FF}) and α, obtained for the two kinds of samples based on FFA and FFB nanoparticles.

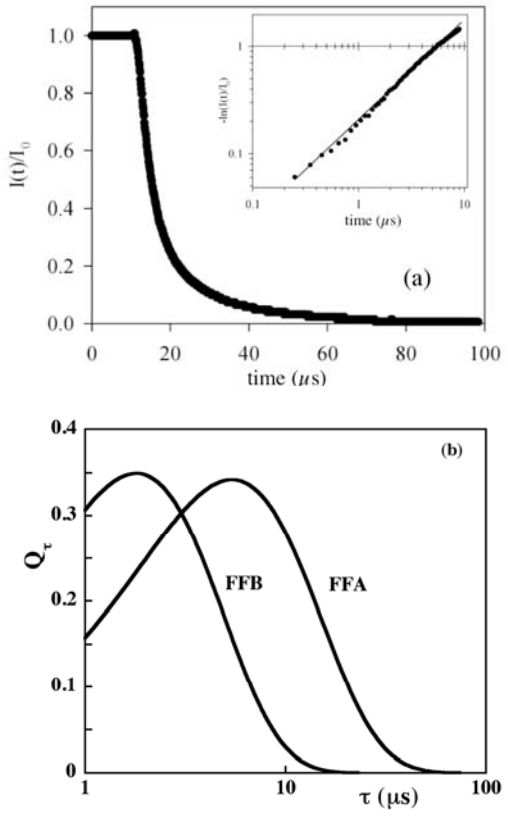

Figure S3 – ***Dynamic birefringence of ferrofluids***

a **–** Relaxation of the optical intensity due to the birefringence of the dispersion under applied magnetic field (FFA with [cit] = 8 10^{-3} mol/L and Φ = 3%). The inset illustrates that the decay is a stretched exponential by plotting $-\ln(I/I_0)$ as a function of time t in a log-log representation.

b – Distribution of characteristic relaxation times for FFA and FFB ferrofluids as obtained from eqn (S13).

In Table S2, the values of α are rather close to 1 but different from 1, it expresses that the relaxation is non-exponential. Such a non-exponential relaxation is usually asserted to the existence of a distribution of times τ inside the ferrofluid. In these liquid solutions it is associated to the polydispersity in hydrodynamic

size of the nanoparticles. This temporal relaxation can be inverted like in [20]. It leads to a distribution $Q(\ln(\tau))$ of relaxation times τ such that:

$$I(t) = \int I_o(\tau) e^{-\frac{t}{\tau}} Q(\ln(\tau)) d(\ln(\tau)) \qquad \text{(S12)}$$

Providing the approximations $I_o(\tau) \approx I_o \approx$ cst for a given sample, $e^{-t/\tau} = 1$ for $t < \tau$ and $e^{-t/\tau} = 0$ for $t > \tau$, it comes [19] :

$$Q(\ln\tau) = -\frac{d(I(t)/I_o)}{d(\ln t)} = \alpha\left(\frac{\tau}{\tau_o}\right)^{\alpha} e^{-\left(\frac{\tau}{\tau_o}\right)^{\alpha}} \qquad \text{(S13)}$$

Figure SI3.b plots these distributions of characteristic times (denoted Q_τ all along this text) for the two kinds of nanoparticles employed here FFA and FFB. Note that in our experimental range of Φ and [Na_3Cit] the obtained distributions are independent of Φ and [Na_3Cit].

3 – Rotational diffusion of nanoparticles within ferrogels probed by dynamical birefringence

Such a dynamical probing may be also performed in ferrogels. Here below the index "FG" stands either for "synth" or "equil" depending on the state of the ferrogel either in the synthesis conditions or at swelling equilibrium.

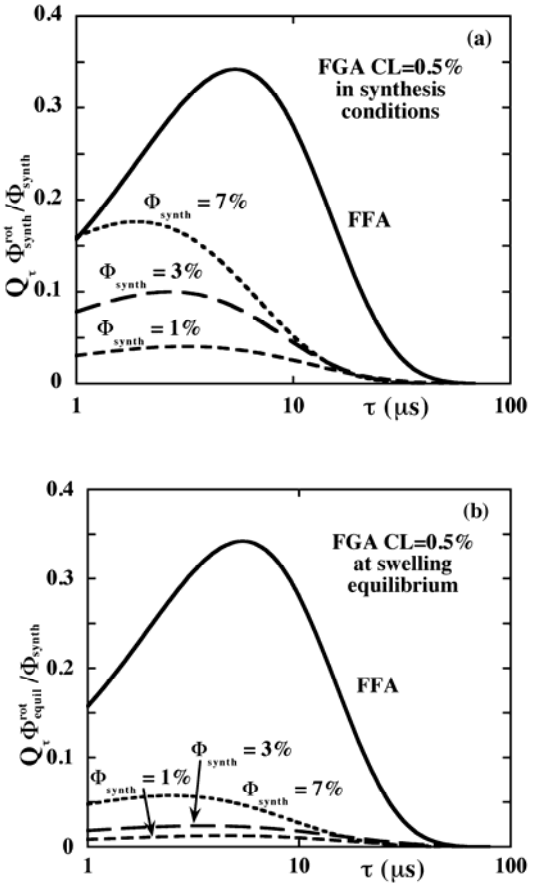

Figure S4 - ***Dynamic birefringence ferrogels FGA - CL = 0.5%*** – Reduced distribution of characteristic times $Q_\tau \Phi^{rot}_{FG}/\Phi_{synth}$ inside ferrogels at various Φ_{synth}, in the synthesis conditions (a) and at swelling equilibrium (b) as compared to pure ferrofluid FFA.

Performing two experiments, one with a ferrogel and one with *its corresponding ferrofluid, at the same volume fraction* $\Phi_{FF} = \Phi_{FG}$ *and with the same sample thickness e*, it is also possible to compare the respective initial intensities I_o^{FG} and I_o^{FF}. I_o^{FG} is here much lower than I_o^{FF} and at most equal to $I_o^{FF}/10$. Using eqns (S10) and (S11), and with the hypothesis that the ratio of magnetic volumes is proportional to the ratio of hydrodynamic volumes, we obtain:

$$\frac{I_o^{FG}}{I_o^{FF}} = \frac{\Phi^{rot}_{FG}}{\Phi_{FF}}\left(\frac{\tau_o^{FG}}{\tau_o^{FF}}\right)^2 \qquad \text{(S14)}$$

Here Φ^{rot}_{FG} is the volume fraction of rotating nanoparticles inside the ferrogel in the low-field experiment of birefringence relaxation. The ratios I_o^{FG}/I_o^{FF} and τ_o^{FG}/τ_o^{FF} being both measured, it is possible using eqn (S14) to deduce $\Phi^{rot}_{FG}/\Phi_{FG}$ the proportion (in volume) of nanoparticles rotating inside the ferrogel in this low field experiment. It is also possible to calculate the volume fraction Φ^{block}_{FG} of nanoparticles blocked in low field using $\Phi^{block}_{FG} = \Phi_{FG} - \Phi^{rot}_{FG}$. They are given in Tables 2, 3 and 5 of main text for the various samples probed here. Figure S4 illustrates for FGA ferrogels at CL = 0.5%, the reduced distributions of characteristic times $Q_\tau \Phi^{rot}_{synth}/\Phi_{synth}$ obtained in non swollen samples at various Φ_{synth} (see Figure S4a) and the corresponding distributions $Q_\tau \Phi^{rot}_{equil}/\Phi_{synth}$ obtained in swollen samples at various Φ_{synth} (see Figure S4b). In these figures, the factors $\Phi^{rot}_{synth}/\Phi_{synth}$ and $\Phi^{rot}_{equil}/\Phi_{synth}$ allow a quantitative visualization of the nanoparticles which are rotating in the ferrogel with respect to those initially introduced.

End-note

(*) A fraction of charged chains could indeed arise from the hydrolysis of the acrylamide monomer into acrylic acid during the synthesis. However, this side reaction of polymerization has been described for PAM hydrogels synthesized at room temperature thanks to the base Tetramethylethylenediamine (TEMED) acting as a catalyst of the persulfate initiator decomposition but also raising the pH (which causes hydrolysis).[21] In our case, we have deliberately chosen to polymerize the hydrogels with thermal initiation at 60°C thus without TEMED. Hence the fraction of charged monomers in the chains of our hydrogels due to spontaneous hydrolysis is estimated below 0.1%, and their effect is visible only by the anomalous swelling ratio of hydrogels in pure water.[8] In the presence of a slight ionic strength (all the experiments of the present article were done in 8mM tri-sodium citrate), this polyelectrolyte effect is screened and therefore we can neglect the ionic contribution to the swelling pressure.

References

[1] L. Benguigui, F. Boué, *Eur. Phys. J. B* **11** (1999) 439
[2] D. Asnaghi, M. Giglio, A. Bossi, P.G. Righetti *Macromolecules* **30** (1997) 6194
[3] Xiaomi Zhang, Zhibing Hu, Yong Li, *Polymer* **39** (1998) 2783-2788
[4] J. Bastide, S. Candau, L. Leibler, *Macromolecules* **14** (1981) 719
[5] A. Hochberg, T. Tanaka, D. Nicoli, *Phys. Rev. Lett.* **43** (1979) 217
[6] T. Hino, J.M. Prausnitz, *J. Appl. Polym. Sci.* **62** (1996) 1635-1640
[7] P.J. Flory, *Principle of Polymer chemistry* (Cornell University Press, Ithaca – NY, 1953)
[8] J.A. Galicia, O. Sandre, F. Cousin, D. Guemghar, C.

Ménager, V. Cabuil, *J. Phys.: Condens. Matter* **15** (2003) S1379
[9] *Polymer Data Handbook* (Oxford University Press, 1999)
[10] Schwartz, T., J. Sabbadin, and J. François, *Polymer* **22** (1981) 609-614
[11] R. Massart, *I.E.E.E. Trans. Magn.* **17** (1981) 1247
[12] R. Massart, E. Dubois, V. Cabuil, E. Hasmonay, *J. Magn. Magn. Mat.* **149** (1995) 1
[13] E. Dubois, V. Cabuil, F. Boué, R. Perzynski, *J. Chem. Phys.* **111** (1999) 7147
[14] F. Gazeau, F. Boué, E. Dubois, R. Perzynski, *J. Phys.: Condens. Matter* **15** (2003) S1305
[15] E. Hasmonay, E. Dubois, J.-C. Bacri, R. Perzynski, Yu. L. Raikher, V.I. Stepanov, *Eur. Phys. J. B* **5** (1998) 859
[16] F. Cousin, E. Dubois, V. Cabuil, *Phys. Rev. E* **68** (2003) 021405
[17] *Magnetic Fluids and Applications Handbook*, ed. by B. Berkovski (Begell House Inc. Publ., New York, 1996)
[18] E. Hasmonay, A. Bee, J.-C. Bacri, R. Perzynski, *J Phys Chem B* **103** (1999) 6421-6428
[19] G. Mériguet, E. Dubois, V. Dupuis, R. Perzynski, *J. Phys.: Condens. Matter* **18** (2006) 10119
[20] C. Wilhelm, F. Gazeau, J. Roger, J.N. Pons, M.F. Salis, R. Perzynski, J.-C. Bacri, *Phys. Rev. E* **65** (2002) 031404
[21] S.I. Takata, T.Norisuye, M. Shibayama Macromolecules **32** (1999) 3989